16th Australasian Fluid Mechanics Conference
Crown Plaza, Gold Coast, Australia
2-7 December 2007

CFD Simulations on the Heating Capability in a Human Nasal Cavity

K. Inthavong, Z.F. Tian, J.Y. Tu
RMIT University, School of Aerospace, Mechanical and Manufacturing Engineering, Victoria 3083 AUSTRALIA

Abstract

The air conditioning capability of the nose is dependent on the nasal mucosal temperature and the airflow dynamics caused by the airway geometry. A computational model of a human nasal cavity obtained through CT scans was produced and CFD techniques were applied to study the effects of morphological differences in the left and right nasal cavity on the airflow and heat transfer of inhaled air. A laminar steady flow of 10L/min was applied and two inhalation conditions were investigated: normal conditions, 25°C, 35% relative humidity and cold dry air conditions, 12°C, 13% relative humidity. It was found that the frontal regions of the nasal cavity exhibited greater secondary cross flows compared to the middle and back regions. The left cavity in the front region had a smaller cross-sectional area compared to the right which allowed greater heating as the heat source from the wall was closer to the bulk flow regions. Additionally it was found that the residence time of the inhaled air was important for the heating ability in laminar flows.

Introduction

A major physiological function of the human nasal cavity is to condition the inhaled air to body core temperature and saturated with vapour to prevent damage to the alveolar epithelium in the lungs. The air conditioning capability of the nose is dependent on the nasal mucosal temperature and the airflow dynamics caused by the airway geometry. Morphological variation of the human nose has been attributed to the eco-geographic adaptation to climate where nasal cavities have been broadly categorised as leptorrhines (tall and narrow) or platyrrhines (short and broad) according to their morphology [16]. It is thought that people exposed to cold dry environments exhibit leptorrhine features that induce turbulent flow features [16],[15]. while those exposed to hot humid environments exhibit platyrrhine features that produce more laminar flow, where the conditioning of the air is less critical [1],[3].

Past experimental studies that have been performed in order to achieve a relationship between nasal morphological features and the flow regime have produced mixed results. For example Proetz [11] and the work by Courtiss and Goldwyn [3] state that the role of the turbinates is to induce turbulence, while Scherer et al. [12] and Elad et al. [4] state that the turbinates laminate the flow by introducing streamlines. The work by Churchill et al. [2] was the first to consider multiple morphological parameters (naris angle, nasal sill height, nasal valve, inferior turbinate and middle turbinate) and its effects on the induction of turbulence at different flow rates. It was found that the projection of the inferior turbinates was the only significant parameter through ANOVA tests and that a greater projection of the inferior turbinate bone laminated the flow by simply decreasing the cross-sectional area of the passageway while larger passageways, with a greater hydraulic diameter, would experience more turbulent flow.

While in-vivo and in-vitro methods provide results that utilise actual realism accounting for physiological changes such as mucociliary clearance and airway obstruction, it also acts as a hindrance through the ability to control such physiological movements. As Lindemann et al. [9] points out, obtaining measurements for the entire nasal airway is technically unrealisable and that in-vivo measurements do not allow for displaying distribution profiles in high resolution as numerical solutions. Computational Fluid Dynamics (CFD) techniques have been used extensively to provide complementary data to existing experimental data. It is an attractive method that is cost-effective, enables enormous amounts of precise data and has the ability to provide deeper insight into the nature of nasal airflow.

Without considering humidity and water exchange, Lindemann et al. [9] numerically simulated the temperature distribution during inspiration in an anatomically realistic nasal cavity. Their simulations used a constant inspiratory flow rate of 2.6 m/s (≈ 25 L/min.) with a constant mucosal wall temperature of 34°C throughout and found that the inspired air (20 °C) was heated to 33.9 °C at the nasopharynx. Compared with in-vivo measurements, the numerical simulation by Lindemann et al. [9] successfully visualized the close relationship between the intranasal air temperature and airflow pattern. Similarly Naftali et al. [10] simulated an unsteady laminar flow using a constant mass diffusivity for the transport of airflow through an idealised cavity model. A periodic inlet of air (25°C, flowrate = 7.5 L/min) was heated by a constant mucosal wall temperature of 37°C. It was found that the simulation produced a higher temperature profile compared with their in-vivo experiments. This may be attributed to the higher constant mucosal wall temperature used, since it was found by Liener et al.[8] that the end-expiratory nasal mucosal wall temperature varied between 32.3°C to 34.7°C after exposure to 25 °C inspired air.

This study highlights the morphological features in the left and right nasal cavity and its effects on the airflow patterns and heat transfer of the inhaled air, under a flow rate of 10L/min. Key geometrical features are identified and its relevance to the heating capacity of the nose is discussed. An anatomically real nasal cavity was used under a steady state case to isolate the air conditioning capability of the nasal cavity independent of the effects of fluctuations.

Model Creation

The nasal cavity geometry was obtained through a CT scan of the nose of a healthy 25 year old, Asian male (170 cm height, 75 kg mass). The CT scan was performed using a CTI Whole Body Scanner (General Electric). The single-matrix scanner was used in helical mode with 1-mm collimation, a 40-cm field of view, 120 kV peak and 200 mA. The scans captured outlined slices in the *x-y* plane at different positions along the *z*-axis from the entrance of the nasal cavity to just anterior of the larynx at intervals of 1 to 5 mm depending on the complexity of the anatomy. The coronal sectioned scans were imported into a three-dimensional (3D) modelling program called GAMBIT (GAMBIT 2.2, 2004) which created smooth curves that connected points on the coronal sections. Stitched surfaces were then created to form a complete computational mesh. Because the details of the flow

velocity and pressure were not known prior to solution of the flow problem, the outlet boundary condition is defined as an outflow with zero diffusion flux for all flow variables in the direction normal to the exit plane. This implies that the flow characteristics have to be consistent with a fully-developed flow assumption and a straight extension of the outlet plane was created into the geometry to satisfy this criterion.

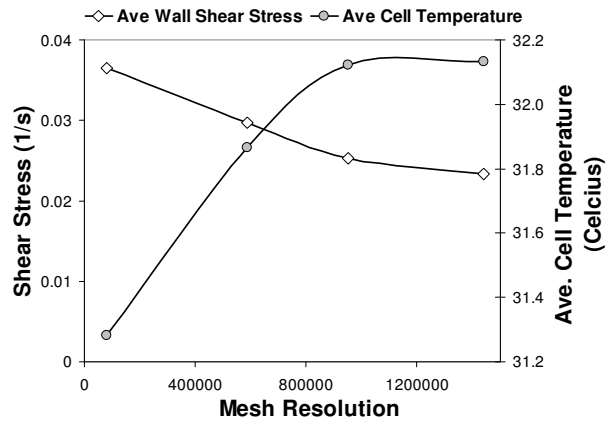

Figure 1. Grid indepence test for the shear stress and the average cell temperature across the entire flow domain.

An initial model with 82,000 unstructured tetrahedral cells was initially used to solve the air flow field at a flow rate of 10L/min. The model was then improved by cell adaptation techniques that included refining large volume cells, cells that displayed high velocity gradients and near wall refinements, where a model with a higher cell count was produced. This process was repeated twice, with each repeat producing a model with a higher cell count than the previous model.

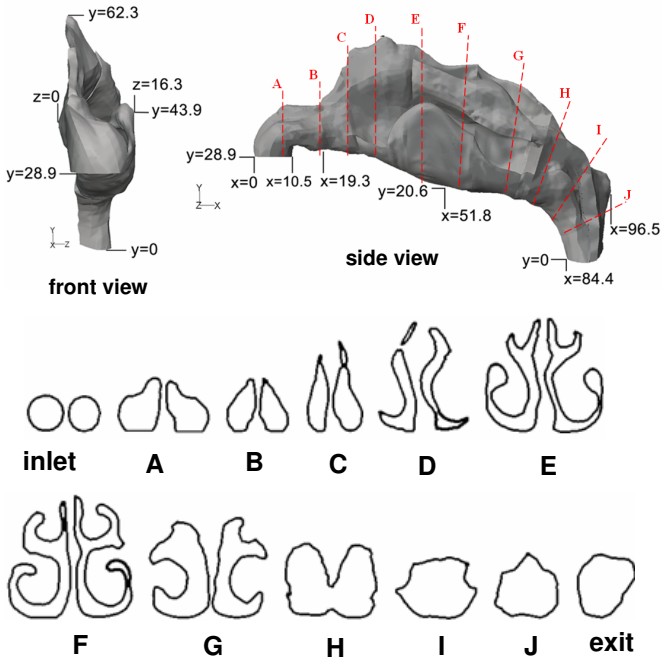

Figure 2. Nasal cavity geometry measurements and the cross-sectional areas used for analysis. The cross-sections are viewed from the front (i.e. looking at a person's face).

Subsequently four models were produced, 82000, 586000, 950000 and 1.44million cells. A grid independence test shown in *Figure 1*, found the results for average cell temperature and the wall shear stress converge as the mesh resolution approached 950,000 cells. In order to make a compromise between the result's accuracy and computational cost, a model with 950,000 elements was used in this study (Figure 2). Note that the convention used to describe the left and right cavities is from the perspective of the frontal view in order to avoid confusion when the cross-sections are displayed. This differs from the anatomical convention where the perspective is taken from the rear view from the back of the person's head.

Fluid Flow Modelling

Due to the complex geometry of the anatomically real nasal cavity a commercial CFD code, FLUENT, was utilised to predict the continuum gas phase flow under steady-state conditions through solutions of the conservation equations of mass and momentum. These equations were discretised using the finite volume approach. The third order accurate QUICK scheme was used to approximate the momentum equation whilst the pressure-velocity coupling was realized through the SIMPLE method. A flow rate of 10L/min. was used to simulate the light adult breathing. At this flow rate, the flow regime has been determined to be laminar [5],[13]. A steady flow rather than a cyclic unsteady flow was used in this case to allow the results to emphasize the effects of airway geometry and the airflow dynamics on the heat transfer independent from cyclic conditions. The steady-state continuity and momentum equations for the gas phase (air) in Cartesian tensor notation are:

$$\frac{\partial}{\partial x_i}\left(\rho_g u_i^g\right) = 0 \tag{1}$$

$$\rho u_j^g \frac{\partial u_i^g}{\partial x_j} = -\frac{\partial p_g}{\partial x_i} + \frac{\partial}{\partial x_j}\left(\mu_g \frac{\partial u_i^g}{\partial x_j}\right) \tag{2}$$

The energy equation is given as:

$$\frac{\partial(\rho u_i E)}{\partial x_i} = \frac{\partial}{\partial x_i}\left(k\frac{\partial T}{\partial x_i} + \mu u_j\left(\frac{\partial u_i}{\partial x_j} + \frac{\partial u_j}{\partial x_i}\right)\right) \tag{3}$$

where

$$E = h - \frac{p}{\rho} + \frac{u^2}{2} \tag{4}$$

h is sensible enthalpy and k is conductivity. The mass transfer equation for water vapor can be written as:

$$\frac{\partial(\rho Y u_i)}{\partial x_i} = -\frac{\partial J_i}{\partial x_i} \tag{5}$$

where Y is the vapor mass fraction and J is the vapor diffusion flux which arises due to concentration gradients. For a laminar flow,

$$J_i = -\rho D\frac{\partial Y}{\partial x_i} \tag{6}$$

The diffusivity D varies with temperature and is expressed by the semi-empirical correlation from Vargaftik [14]:

$$D = 2.16e^{-5}\left(T/273.15\right)^{1.8} \tag{7}$$

which was implemented into a commercial CFD code FLUENT through the user-defined functions.

Boundary Conditions

A total mass flux inlet condition of 10L/min. was applied at the nostril openings. Two climatic conditions were used for the inspired ambient air; normal air conditions (25°C, 35% relative humidity) and a cold dry condition, (12°C, 13% relative humidity). The inner mucosal walls which are covered by a wet mucus layer are assumed to be fully saturated with water vapour and have an unlimited supply of heat and water. Liener et al. [8] were able to measure local nasal mucosal wall temperatures after exposure to air at different climatic conditions, which ranged from 32.3°C – 34.7°C for normal air conditions and 30.6°C – 33.7°C for cold dry air. Therefore a value of 33.5°C and a value of 32.1°C was applied for the normal air and the cold dry air case respectively.

Results and Discussion

Temperature Profiles

The temperature profiles were obtained from the averaged temperature at each cross-section throughout the airway for a breathing rate of 10 L/min. The results for the normal air condition were compared with experimental work by Keck et al. [6],[7] whose results were averaged from a population of 50 and 23 volunteers respectively. The profile showed good agreement in the frontal regions of the nasal airway, while a small discrepancy is observed in the back regions towards the nasopharynx. The profile converged to a steady value at a distance of 40mm from the inlet, suggesting that the air is conditioned early in the front region.

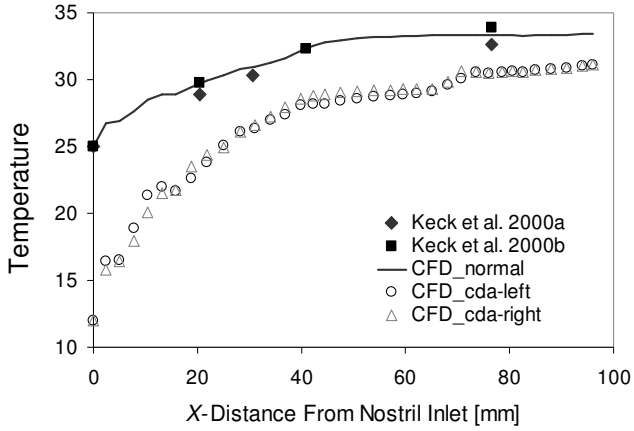

Figure 3. Temperature profiles across the nasal cavity from the inlet. The solid black line represents a normal inhalation condition compared with experimental work. The un-colored symbols represent the simulated results for cold dry air.

The profiles for the inhalation of cold dry air were recorded for the left and right sides of the nasal cavity and also shown in Figure 3. The temperature profiles converge to a peak value of 30.7°C for the last ten measurements away from the inlet. This compares with the inhalation of normal air which has a value of 33.3°C for the last ten measurements. The distance at which the profile converged to a steady value is 71mm from the inlet which is the location where the left and right cavities begin to merge together.

For normal air conditions, heating of the air is dominant in the frontal region of the airway. The temperature difference is stable after the anterior turbinate region and the heat transfer is minimal. One of the roles of the highly vascularised turbinate region that has been widely discussed is to condition the inhaled air. However in the case of normal air conditions, the turbinate region does not actually apply much heat transfer but rather acts as a heat source through its constant temperature maintained by the underlying capillary bed on the mucosal surface that provides the walls with this energy. The majority of the temperature increases occurs in the frontal regions where the temperature difference is greatest. For the cold dry air case, the temperature profile follows a similar curve, but shifted downwards to accommodate the temperature decrease.

Airflow in Left and Right Cavities

The effects of the airflow dynamics due to the asymmetry of the left and right side of the cavity is shown in Figure 4 which combines the contours of the axial velocity (*x*-component of velocity) with streamlines of secondary flow (*y*-*z* component of velocity).

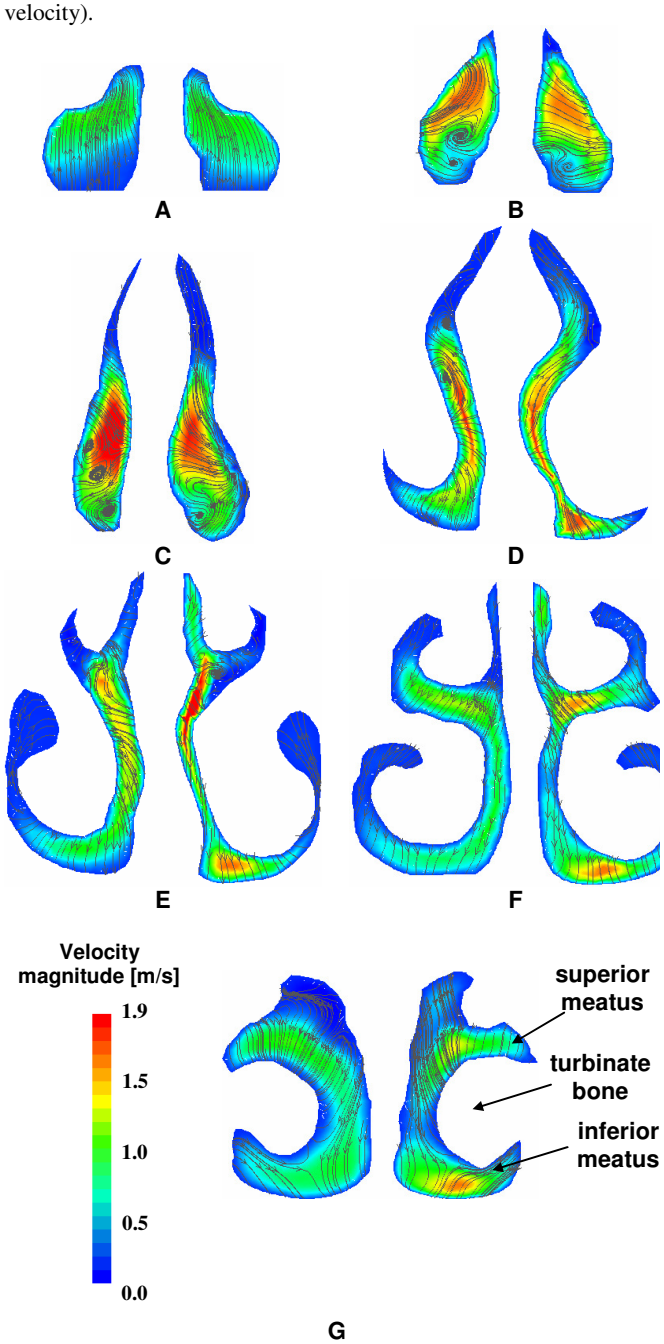

Figure 4 Comparison of the left and right cavities showing contours of axial velocity (x-direction) and streamlines of cross-flow (y-z direction). Red contours represent maximum values while blue represent minimums.

The red contours suggest the main flow field since the direction of flow is in the *x*-axis and therefore the blue contours show low flow in the *x*-axis. At the beginning of the flow at *A*, air flows upwards as shown by the streamlines pointing in the positive y direction. No cross flow in the *z*-direction is found. The flow

accelerates at *B* as the airway decreases in area where the nasal valve region begins to form. At this cross-section, the flow has changed directions about 90° from the inlet and coupled with the narrower region, cross flows in the *y* and *z* directions are more prevalent especially in the left side. Additionally the flow begins to split into two directions with the majority flowing upwards and a smaller proportion flowing downwards.

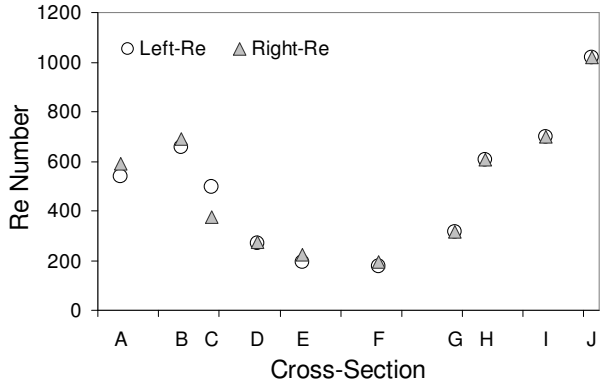

Figure 5. Reynolds number recorded at the cross-sections depicted in figure 2. The cross-sections have been scaled to reflect their relative distances from each other across the nasal cavity. The axial distance is 0-90mm.

The geometry continues to become thinner and this accelerates the bulk flow through the middle of *C*. The flow away from the centre is found to be moving away from the septum walls and pushing upwards and downwards coinciding with the geometry which is expanding vertically. This flow feature continues through *D* as the meatus forms. At the turbinate region *E,F,G* the main axial flow remains close to the septum walls and little flow reaches the outer meatus region. As the geometry begins to curve downwards, the flow streamlines reflect this by pointing in the negative *y*-direction.

LEFT	Area (mm^2)	Hyd Diam. (mm)	Velocity
A	67	7.6	1.06
B	65	7.7	1.29
C	93	7.0	1.08
D	140	5.2	0.79
E	180	5.5	0.53
F	216	5.9	0.46
G	248	11.0	0.43
RIGHT	**Area (mm^2)**	**Hyd Diam. (mm)**	**Velocity**
A	76	8.3	1.09
B	74	8.4	1.24
C	105	7.1	0.80
D	119	4.9	0.85
E	147	4.8	0.70
F	184	6.3	0.47
G	193	10.5	0.46
COMBINED	**Area (mm^2)**	**Hyd Diam. (mm)**	**Velocity**
H	551	22.5	0.41
I	338	16.0	0.66
J	230	16.2	0.95

Table 1. Velocity magnitude and geometrical details of the cross-sections depicted in figure 2.

Comparisons of the Reynolds number showed that both cavities exhibited similar values, except in the front regions of the airway especially at section C (*Figure 5*). The left cavity has a higher value, Re = 496 compared with the right cavity, Re = 376. It was found that the large difference between the cavities at section C was due to the greater velocity in the left cavity (Table.1). Although the hydraulic diameters were similar, the cross-sectional area of the right-side is greater than the left-side. This suggests that the left-side has a narrower cross-section compared to the right-side which causes the airflow to accelerate and hence increases the Reynolds number. In the turbinate regions at sections E, F and G, there are some differences in the airway geometry as well as the flow velocity. The right side experiences a greater velocity due to a narrower cross-section which produces a higher Reynolds number.

Temperatures in Left and Right Cavities

Given that other dependent variables, such as wall temperature and a steady air flow were kept constant in this study, the effects of the differences in nasal morphology and hence the differences in the flow field could be isolated for analysis. The averaged temperatures at different cross-sections shown in *Figure 6* were recorded and compared. The left cavity produces higher temperatures in the front regions before the airway expands just after cross-section B ($x \approx 19$mm), however after the airway expansion the right cavity produces higher values.

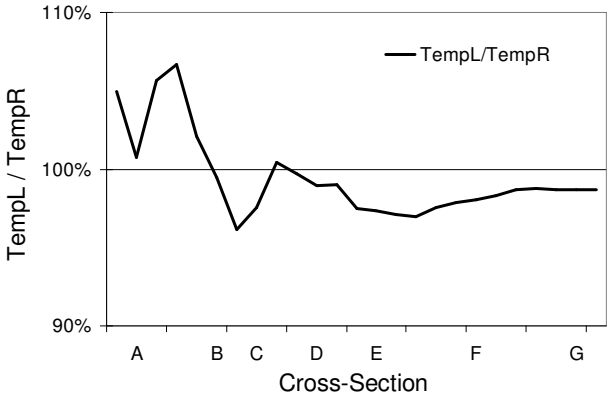

Figure 6. Ratio of the average temperature across the cross-sections of the left cavity with the average temperature across the cross-section of the right cavity.

The contour plots reveal that the cooler air is found at the central locations of each cross section furthest from the wall. The temperatures at the olfactory regions (top of section *D,E*) remain high as there is little airflow that reaches this upper region and the region is heated by the close surrounding walls. This is an important feature of the human body as the olfactory epithelium is lined with delicate olfactory receptor neurons which need to be void of any cold dry air exposure to prevent any damage. At section *C*, the left-side is thinner; however the bulk of the flow remains in the middle region which accelerates through.

The bulk flow regions are the last to be heated up to a peak value of 30.7°C. A comparison of the temperature contour plots in Figure 7 with the axial velocity contours in Figure 4 shows that at high axial velocity regions, the temperature is at its lowest. This is due to the finite heat source provided by the constant wall temperature where the heating of the cold air is dependent on the mass flow rate as depicted by the thermodynamic balance equation:

$$\dot{q} = \dot{m} C_p \left(T_{wall} - T_{air} \right) \quad (8)$$

This implies that the flow residence time, $\dot{m}$ is critical for the inhaled air to be heated, given that the heat source is driven by

the difference in the constant wall temperature and the inhaled air.

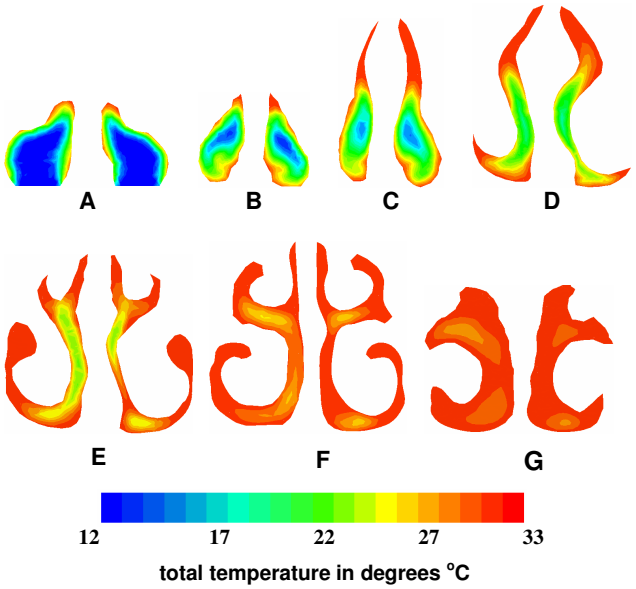

Figure 7. Contours of total temperature at cross-sections throughout the nasal cavity.

Wall Heat Flux

The wall heat flux was mapped for the entire airway however only the region up to section *F* is shown since the region thereafter showed little change. The heat flux is greatest at the frontal regions where the temperature gradients are greatest. The lower and upper sections of the airway exhibit low fluxes if any since the flow of the inhaled air is minimal in those regions. At the anterior turbinate region the protruding meatus regions do not show any heat flux.

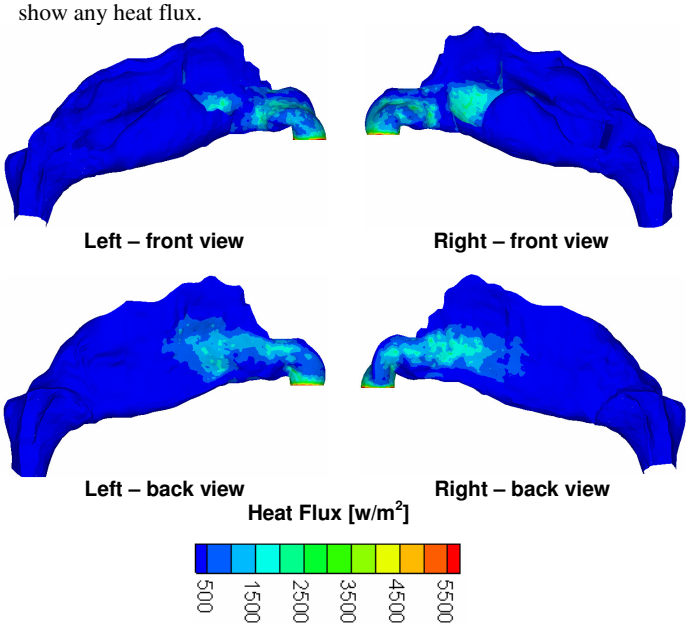

Figure 8. Wall heat flux for a cold dry air condition.

However the main airway attached to the septum walls show that heat is being transferred. The region after the anterior turbinates show no heat flux which means that the surrounding air adjacent to the walls has reached body core temperatures. Further heating becomes dependent on the airflow dynamics especially for the air which requires convective movements to enhance heat transfer. An increase in the velocity magnitude will not necessarily enhance the heat transfer due to the shorter residence time, but rather an increase in the cross-flow in the y-z directions is required to promote mixing and the convective heat transfer.

Conclusions

Temperature profiles of inhaled normal air conditions at 25°C, 35% relative humidity showed that the capacity of the nasal cavity to heat cold inhaled air to body core temperature is achieved profile converged to a steady value a value of 33.3°C at a distance of 40mm from the inlet, suggesting that the air is conditioned early in the front region. This compared with the inhalation of cold dry air 12°C, 13% which reached a value of 30.7°C and converged later at a distance of 71mm from the inlet.

It was found that in the frontal regions where the flow changes direction, the flow contained more secondary flow features such as vortices in the *y-z* directions. The flow rises in the frontal regions and after the anterior turbinate regions begins to fall due to the nasal cavity geometry. The cross-flow in the z-direction is not as evident in the back regions of the airway.

The differences in the width of the airway especially in the frontal regions was found to be critical as the temperature difference was the greatest and therefore heating of the air is expedited when the air is surrounded by the hotter walls. As the temperature rises the effects of the wall on the bulk flow is less prominent as the heat needs to diffuse through the boundary layer which is now bigger. The temperature difference between the air flow adjacent to the walls is now smaller and convective heat transfer becomes important. The air temperature in the left side was found to be hotter in the frontal regions where the airway was thinner and had a smaller cross-section compared with the right side. After the airway expansion the opposite trend occurred as the right side became warmer than the left side due to a smaller cross-sectional area.

This study was able to show the morphological differences in the left and right nasal cavity and the effects it had on the airflow and the heat transfer to the inhaled air. Further studies are being investigated on the role of the turbinates on the heating capability of the airflow under turbulent features.

Acknowledgments

The financial support provided by the Australian Research Council (project ID LP0561870) is gratefully acknowledged.

References

[1] Carey, J.W., & Steegmann, A.T.J., Human Nasal Protrusion, Latitude, and Climate, *Am. J. Phys. Anthropol.*, **56**, 1981, 313–319.

[2] Churchill S.E., Shackelford L.L., Georgi J.N., and Black M.T., Morphological Variation and Airflow Dynamics in the Human Nose, American Journal of Human Biology, **16**, 2004, 625–638.

[3] Courtiss, E. H., & Goldwyn, R.M., The Effects of Nasal Surgery on Airflow, *Plastic. Reconstr. Surg*. **72**, 1983, 9–19.

[4] Elad, D., Liebenthal, R., Wenig, B.L., & Einav, S., Analysis of Air Flow Patterns in the Human Nose, *Med. Biol. Eng. Comp*., **31**, 1993, 585–592.

[5] Hahn, I., Schere, P. W., & Mozell, M. M., Velocity Profiles Measured for Airflow Through a Large-scale Model of the Human Nasal Cavity, *J. Appl. Physiol*., **75**, 1993, 2273–2287.

[6] Keck, T., Leiacker, R., Riechelmann, H., & Rettinger, G., Temperature Profile in the Nasal Cavity, *Laryngoscope*, **110**, 2000, 651-654.

[7] Keck, T., Leiacker, R., Heinrich, A., Kuhneman, S. and Rettinger, G, Humidity and Temperature Profiles in the Nasal Cavity, Rhinology **38**, pp.167-171, 2000

[8] Lienar, K., Leiacker, R., Lindemann, J., Rettinger G., & Keck, T., Nasal Mucosal Temperature after Exposure to Cold, Dry Air and Hot, Humid Air, *Acta Otolaryngol*., **123**, 2003, 851-856.

[9] Lindemann, J., Keck, T., Wiesmiller, K., Sander, B., Brambs, H.J., Rettinger, G., & Pless, D., A Numerical Simulation of Intranasal Air Temperature during Inspiration, *Laryngoscope*, **114**, 2004, 1037-1041.

[10] Naftali, S., Rosenfeld, M., Wolf, M., & Elad, D., The Air-Conditioning Capacity of the Human Nose, *Annals of Biomed. Eng*., **33**, 2005, 545-553.

[11] Proetz, A.W., Air Currents in the Upper Respiratory Tract and Their Clinical Importance, *Ann. Otol. Rhinol. Laryngol*., **60**, 1951, 439–467.

[12] Scherer, P.W., Hahn, I.I., & Mozell, M.M., The Biophysics of Nasal Airflow, *Otolaryngol. Clin. N. Am.,* **22**, 1989, 265–278.

[13] Swift, D.L., Proctor, D.F., Access of Air to the Respiratory Tract. In Brain, J.D., Proctor, D.F. and Reid, L.M. (eds), Respiratory Defence Mechanisms. Marcel Dekker, New York, NY, pp.63–93 1977.

[14] Vargaftik, N. B., Tables on Thermophysical Properties of Liquids and Gases, 2nd Ed., Washington, DC: Hemisphere, 1975.

[15] Weiner, J.S., Nose Shape and Climate, *Am. J. Phys. Anthropol*., **12,** 1954, 615–618.

[16] Wolpoff, M. H. Climatic Influence on the Skeletal Nasal Aperture, *Am. J. Phys. Anthropol*., **29**, 1968, 405-424.